M.L. Stone and J.R. Anderson

Advances in Primary-Radar Technology

Current primary radars have difficulty detecting aircraft when ground clutter, rain, or birds interfere. To overcome such interference, the Moving Target Detector (MTD) uses adaptive digital signal and data processing techniques. MTD has provided the foundation for a new generation of primary radars called Airport Surveillance Radar-9 (ASR-9). In addition to achieving near-optimal target-detection performance, ASR-9 also provides timely weather information. The Federal Aviation Administration (FAA) is installing ASR-9 systems at more than 100 airports across the United States.

While the role of beacon (or secondary) radars in air traffic control is growing, there is a continuing need for primary radar in providing aircraft position data. In addition to aircraft surveillance, primary radars provide air traffic controllers with timely weather information that can be used to direct airplanes flying in or near hazardous weather.

Originally, primary radars were magnetron systems equipped with a single fan-beam antenna mounted on an azimuth rotator. Later versions incorporated Moving Target Indicator (MTI) detectors, which used delay lines to cancel ground clutter. MTI radars, however, have difficulty detecting aircraft when ground vehicles, rain, or birds interfere.

To handle such adverse conditions, the Airport Surveillance Radar-9 (ASR-9) [1], a next-generation primary radar, uses the Moving Target Detector (MTD) [2–4] concept. MTD employs several adaptive digital signal and data processing techniques. For example, Doppler processing eliminates ground and rain clutter. Doppler processing is followed by a number of target editing steps; e.g., a ground-clutter map rejects false alarms that result from mountains and buildings. In another instance, fixed and area (adaptive) thresholds eliminate echoes caused by flocks of birds or clutter due to vehicular traffic such as automobiles and trucks. MTD achieves further reduction of false alarms with a surveillance-processing module that uses scan-to-scan correlation for rejecting

targets that fail to meet spatial or temporal criteria. As a result of MTD processing steps on equipped radar, ASR-9 can deliver, via telephone lines, a set of target reports free of the clutter and false alarms found in earlier airport primary radars.

ASR-9 also has a separate weather channel that provides concise and timely reports on storm intensities and positions. An air traffic controller can select and display any two of six National Weather Service (NWS) intensity levels to obtain an accurate representation of the location of any storms that might be hazardous to aircraft.

The MTD processor architecture was developed during the 1970s under Federal Aviation Administration (FAA) sponsorship by a Lincoln Laboratory team [2–6]. The team, led by C.E. Muehe, chose a technique that used block-staggered groups of pulses to detect any targets masked by intense rain clutter. Initially, the team constructed and field-tested a hard-wired (nonprogrammable) system. A parallel micro-programmed processor (PMP) version called the MTD-II followed in the late 1970s. PMP [7, 8] facilitated MTD's ability to adapt to different environments, a feature deemed necessary to optimize the system's performance at a variety of sites. Subsequent tests of the MTD-II processors in challenging environments demonstrated two benefits: reliable, essentially clutter-free detection; and a reduction in the false-alarm rate superior to that attained by earlier radars

(a)
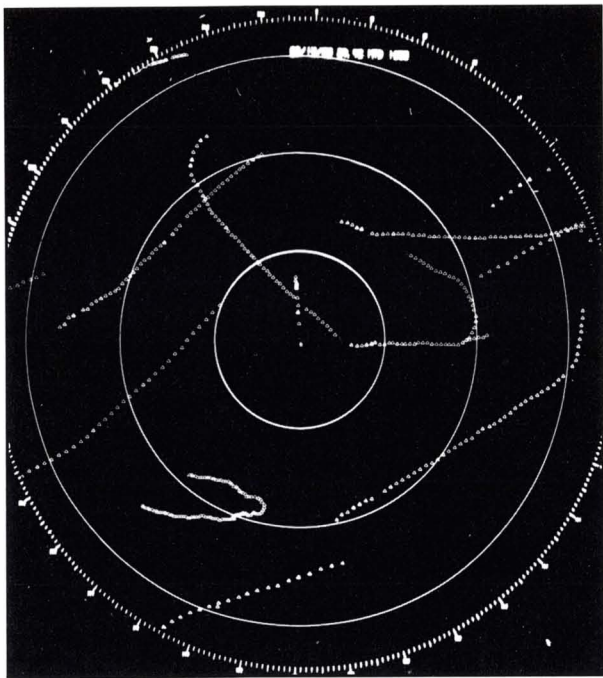
(b)

Fig. 1—Detection of aircraft flying in rain. (a) Output of a conventional MTI radar taken with a 5-min exposure. The aircraft flying within the rain echoes is obscured. (b) Output of moving target detector (MTD). The screen is free of rain clutter and the overall track of the aircraft is clearly delineated. Because only one display was available, the photographs were made sequentially.

[9, 10]. Figure 1 gives a qualitative illustration of the superiority of MTD over MTI in detecting aircraft flying in rain.

MTD and the weather channel used in ASR-9 represent a significant improvement in primary-radar technology. The FAA is installing ASR-9 systems at more than 100 major airports in the United States (Fig. 2). This article first delineates the primary-radar requirements for aircraft and weather surveillance. Next, MTD is described and the system's test results are discussed. Finally, we comment on possible future enhancements to the MTD concept.

Performance Requirements for Airport Primary Radars

Table 1 gives the performance requirements of an airport primary radar. The requirements, which are embodied in our current MTD model, place extreme demands on primary-radar performance. It is essential that a primary radar

- reject ground clutter by at least 40 dB,
- continue to perform in the presence of rain,
- adapt to limit the false-target reports generated by birds and vehicular traffic such as automobiles and trucks, and
- eliminate any additional clutter breakthrough by means of scan-to-scan processing.

Moving Target Detector

The main improvements of MTD over its predecessor, MTI, are that MTD performs clutter mitigation by means of digital Doppler filter processing and the use of false-alarm-rate thresholds. Other adaptive features of MTD eliminate bird echoes and vehicular traffic. The overall processing reduces the output to telephone-line bandwidth.

Figure 3 shows a block diagram of the MTD system, which includes a dual fan-beam elevation antenna (Fig. 4). Transmission takes place through the lower beam. The upper beam receives echoes at close range, which reduces the strength of the echoes that result from ground clutter. The lower beam is used for distant targets; its minus 3-dB point is typically di-
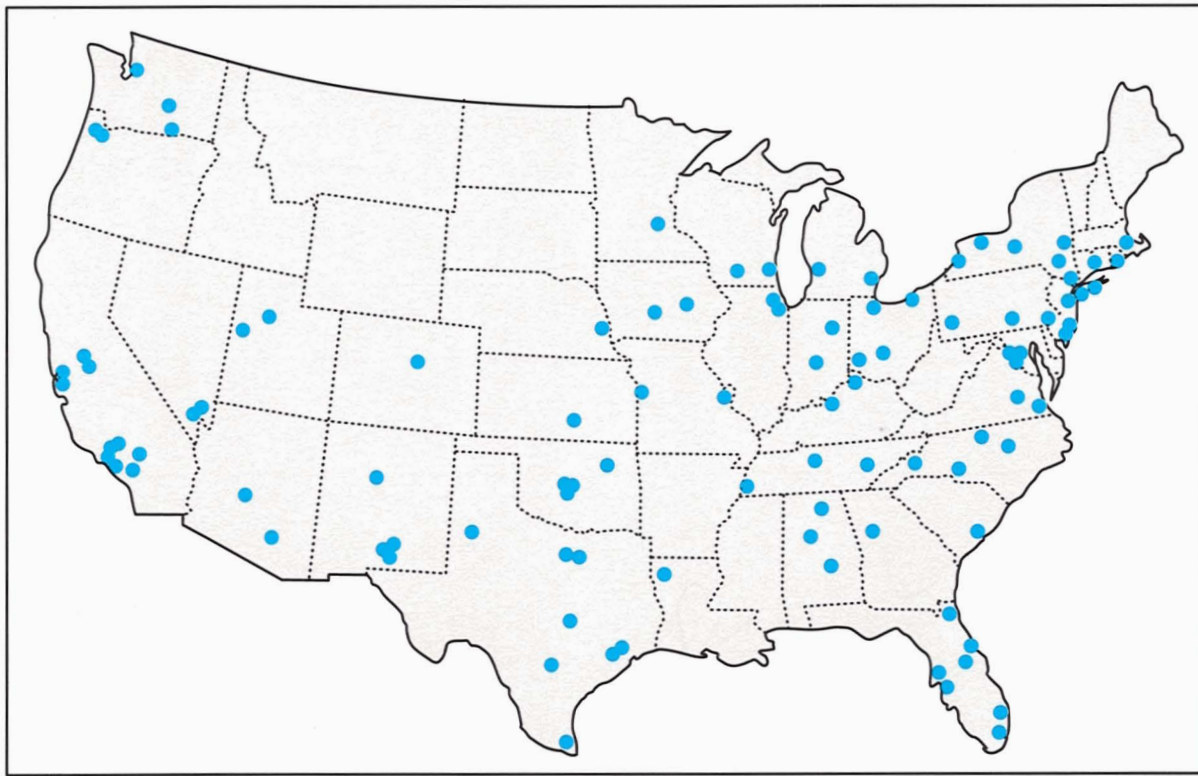
Fig. 2—Planned ASR-9 installations in the United States.

rected toward the horizon.

Although the antenna normally both radiates and receives vertical polarization, whenever there is heavy precipitation over a significant portion of the coverage area, the radar switches to circular polarization. By doing so, the sensor achieves an additional 12 to 20 dB of precipitation-echo rejection. During the time that circular polarization is used, weather signals are derived from the orthogonal-polarization ports

---

Table 1. Surveillance Requirements for MTD-Based Airport Primary Radars

- Maximum range = 60 nmi.
- Altitude coverage = 0 ft to 25,000 ft.
- Update rate = 4.8 s.
- Probability of detecting a small aircraft = 0.9.
- False-alarm rate at the output of a tracking filter = 1 per scan.
- False-alarm rate at the output of the correlation and interpolation filter = 20 per scan.
- Range accuracy = 1/32 of a nautical mile with a 200-ft rms.
- Azimuth accuracy = 0.16° rms.
- Capacity = 400 aircraft distributed nonuniformly in azimuth.
- Weather reporting: six National Weather Service (NWS) levels are available for pairwise selection by the air traffic controller.
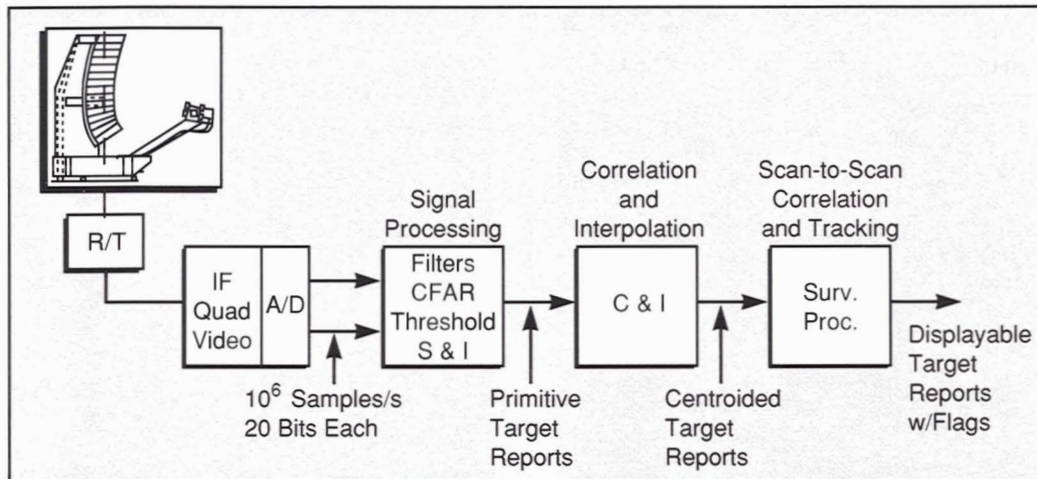

Fig. 3— MTD-II block diagram.

of the antenna. Meanwhile, the target signals are received through the same ports of the antenna that are used when linear polarization is radiated. Multiple-channel rotary joints carry the information of the received signals to the processing units, which are located in a shelter at the base of the antenna tower. During operation with circular polarization, a switch located on the antenna selects either the weather-channel upper or lower beam. The signal from the selected beam is then passed through a single rotating joint to the weather-channel receiver.

Signals for target detection pass from the antenna through a sensitivity time control and a low-noise amplifier. After the signals are heterodyned to an intermediate frequency, they are translated to baseband at the output of a linear receiver. This step provides in-phase and quadrature video signals, which A/D converters sample.

There are two coherent processing intervals (CPI) for each beam dwell, and each beam dwell commences in synchronism with a bearing pulse from the shaft encoder that reports the antenna's position. In the case of ASR-9, the individual CPIs in the CPI pair use 8 and 10 pulses, respectively, with a nominal average pulse-repetition frequency (PRF) of 1,000 Hz and a nine-to-seven ratio between the two CPIs. Fill pulses account for variations in the angular rate of the antenna that result from wind effects.

For each of the 8 or 10 CPI periods, the pro-

cessor's input memories store the signals for the 960 range gates, which span 60 nmi. The processor then performs saturation and interference testing of the digital signals, followed by Doppler filtering and thresholding. Finally, range, azimuth, Doppler amplitude, and quality values are delivered for the targets in the range cells that contain detections. (A quality value [11] indicates the expected azimuth estimate error.) A detection occurs whenever a threshold is crossed in a particular range cell of roughly 150 m. The detections are then correlated and interpolated; i.e., the reports are correlated and centroids are found for the range and azimuth measurements. After the reports are subjected to additional criteria for false-alarm rejection, they are passed to a scan-to-scan correlator that reduces the output false-alarm rate to about one per scan.

The MTD Processor

The MTD processor performs several functions: signal processing, thresholding, post-detection processing, area thresholding, and scan-to-scan correlation.

Signal Processing

MTD's central functional element is a set of Doppler filters, typically 8 or 10 for each range cell or sample. The output of the filters are all individually subjected to thresholds [1, 12]. The

input to the filters is derived from the output of the quadrature video detectors, which are sampled by two 12-bit A/D converters operating at a rate of 1 MHz. For each 4.8-s revolution of the radar antenna, there are 256 azimuth beam dwells, each of which contains two CPIs. For each CPI, 960 range cells are processed. Thus, after every revolution of the antenna, more than 4 million Doppler filters are formed. The output signals of the Doppler filters are examined by the signal processor, which uses threshold criteria appropriate to the desired false-alarm rate and to the locations of the signals relative to several factors: ground clutter, precipitation echoes, and the number of bird echoes encountered.

To obtain acceptable performance in conditions of rain- and ground-clutter interference, the developmental model of MTD used a set of eight finite impulse-response filters for each range cell. Two pulse-repetition intervals were used to prevent the masking that occurs when rain clutter obscures a target. (Masking can also result when the target Doppler frequency is a near integer multiple of the PRF.)

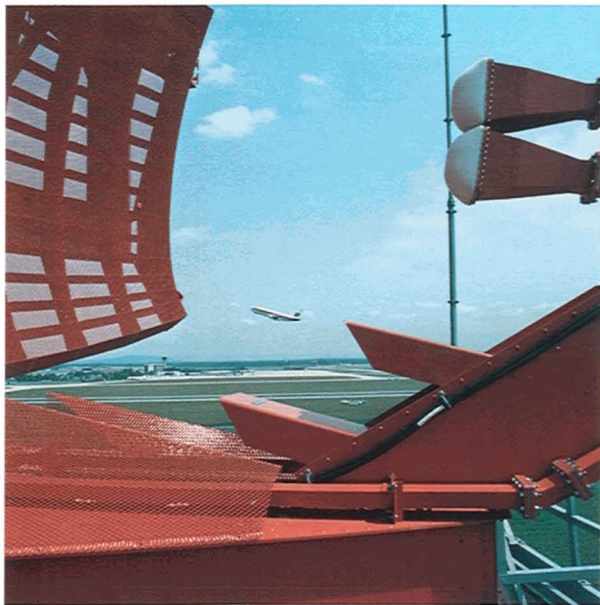As noted, the filter design in ASR-9 employs

Fig. 4— ASR-9 antenna. Networks used to change the antenna's polarization from linear vertical to circular have been installed adjacent to the two feed horns that form the upper and lower beams. (Photo courtesy of Westinghouse Electric.)

either 8 or 10 samples of 12-bit words to improve the system's detection at ranges affected by ground clutter. Optimum filter characteristics were obtained by making the time span of the CPIs equal; i.e., 8 pulses were used at a low repetition rate and 10 pulses were used at a high repetition rate.

Thresholding

Primitive target reports are declared from the output of the filters after the data are subjected to certain thresholds. (The targets are called primitive because they have not yet been associated with other criteria.)

The output of the zero-velocity filter is subjected to a threshold value equal to the single-pole average of the clutter values that were observed in the subject range cell over 10 to 20 scans. The values are updated every other scan. The thresholding processor uses a multiplier to attain a false-alarm rate on the order of 10^{-5}.

A sliding-window, constant false-alarm rate (CFAR) threshold is used to determine the range thresholds for the nonzero-Doppler-velocity filters. The CFAR processor calculates a threshold by averaging the six cells preceding and seven cells following an interval that includes the range cell under test and the two adjacent cells immediately preceding and following that range cell. (Thus the total window, which is approximately 1 nmi long, includes 16 range cells.) Appropriate adjustment is made to achieve a 10^{-5} false-alarm rate. In range cells affected by severe ground clutter, the CFAR threshold is increased by a fraction of the zero-filter output. The goal of the CFAR processor is to achieve a rate of 60 to 100 false alarms per scan.

To improve the system's ability to distinguish between two neighboring targets with similar Doppler velocities, ASR-9 uses a more sophisticated algorithm than the original version of MTD. (Whenever targets were separated by less than 0.5 nmi, the MTD-II algorithm had a low probability of resolving them [1].) In determining the interference level used for the threshold, the ASR-9 CFAR algorithm eliminates the three strongest samples within the CFAR window. A *greater of* criterion is also employed to choose

between the interference power of the preceding and following groups of range cells adjacent to the cell under test. Analysis indicates that this algorithm, which Westinghouse Electric Corp. developed, can resolve targets as close as 0.25 nmi.

Post-Detection Processing

Using post-detection processing, we can reduce the aforementioned false-alarm rate to one false alarm per scan when averaged over a 10-scan interval. In post-detection processing, thresholded target reports are subjected to additional filtering. The filtering removes ground clutter that exceeds the design characteristics of the filter bank. A high-spatial-resolution map (0.25 nmi × 2.8°) is employed to select the appropriate threshold values: for the ground clutter, a Doppler weighting that corresponds to the scanning modulation; and, for the ground traffic, a flat-topped Doppler weighting. After this operation is completed, the reports are correlated and interpolated.

In MTD, targets are grouped in accordance with their spatial adjacency (Fig. 5). The centroids of the different groups are then calculated from a center-of-mass estimation (first moment weighted by amplitude). Each centroided target report is given a quality value: an integer ranging from 0 to 3 that indicates the number of detections that were made as the antenna scanned past the target. A high quality value corresponds to a greater number of detections. The MTD tracker uses a target's quality value as one of the criteria in deciding whether the target should be ignored, entered to update a track, or pursued to initiate a new track during the next scan.

The ASR-9 design enhances azimuth resolution by employing a beam-matching algorithm. When a run of reports extends beyond two beamwidths, ASR-9 compares the amplitude data with a pattern that a large single target would produce. A substantial difference between the amplitude data and the expected pattern implies the existence of two targets in close azimuthal proximity [1].
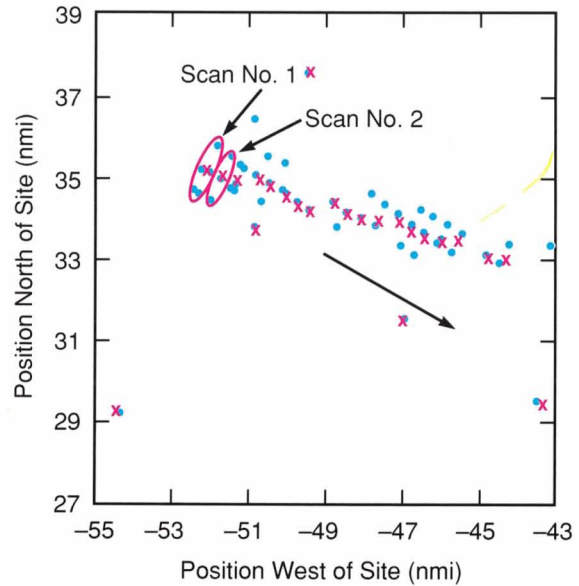

Fig. 5—Targets are grouped in accordance with their spatial adjacency. The centroids of the target groups are then calculated and plotted (shown as xs).

Area Thresholding

The sensitivity of MTD-II permits the detection of birds and insect targets that have mean cross sections of approximately 0.003 m^2 and effective radar-backscattering cross sections as small as 0.001 m^2. In comparison, aircraft targets have apparent mean cross sections of 1 m^2. Figure 6 gives an example of the distributions of these two types of populations, as observed in Burlington, Vt. [12]. In the figure, the two population types in the region between –10 dBsm and 0 dBsm overlap. Because of the overlap, it is impossible to determine unequivocally whether a single report is due to an aircraft or a bird on the basis of amplitude information only.

The area-thresholding process reduces the effects of bird populations by limiting the false-alarm rate to a fixed maximum value that has as small an effect on the detection rate as possible. The threshold is set by integrating reports for the time necessary to obtain an accurate estimate of low cross-section target detections. If the count exceeds a nominal value of 60 false alarms per scan over the coverage area, the area-thresholding processor raises the thresholds.

The tendency of bird flocks to take to the air

en masse and our desire to accumulate representative and stable target statistics require the use of two filters in MTD-II's area-thresholding processor. The first filter integrates over 200 s with approximately $16 \, \text{mi}^2 \times 3$-Doppler-bin resolution. The second filter integrates over 5 s and covers within 20 mi of the radar and within 3 Doppler bins. The two-filter combination mitigates, on a localized basis, the effects of long-lasting bird flights. At the same time, the filter combination can respond quickly to cope with the sudden flight of a flock of birds. Figure 7(a) and (b) give an example of the effectiveness of MTD-II's adaptive thresholding in coping with echoes from birds. Figure 7(a) gives an example of bird echoes that were observed prior to area thresholding. The effectiveness of MTD-II's area thresholding in coping with bird echoes is illustrated in Fig. 7(b).

Scan-to-Scan Correlation (Tracking)

Targets that pass the area-thresholding criteria are then subjected to a tracking filter. The tracking filter removes those targets or false alarms which do not have a scan-to-scan relationship appropriate to the projected position of an aircraft target.

The tracking algorithm initially associates a track with a target on the basis of the target's normalized error distance from its predicted position. Targets associated for two scans are transmitted to the display. The quality value carried by a target report is used to determine the amount of smoothing done by the tracker's azimuth-predicting algorithm. After three consecutive scans, a track that is not matched with a target is dropped. Unmatched targets are retained for one scan so that they can help initiate new tracks. Although the tracking processor does not place a low-velocity limit on the tracks, MTD-II suppresses targets that correlate with tracks but that never move more than 0.25 mi from their initial track positions. This feature is optional in ASR-9.

The result of MTD-II's overall surveillance processing is the generation of output reports on more than 98% of aircraft-target detections while the processing limits the false-alarm rate to less than one false alarm per scan under nominal conditions.

Performance

In 1975 a hard-wired version of MTD was evaluated at the FAA Test Center in Atlantic City, N.J. The tests demonstrated the efficacy of the MTD concept but led to the conclusion that a programmable processor was necessary to facilitate maintenance and the adjustment of site-variable parameters. (The parameters are required to mitigate the effects of site-specific conditions that lead to false alarms, e.g., bird clutter, road traffic, and the presence of physical objects such as buildings and hills.) Consequently, a PMP-based version, the MTD-II, was assembled and tested at two locations: the FAA Test Center, which presented a challenging bird-clutter environment; and the site at the Burlington, Vt., airport, which provided extremely high clutter conditions. Subsequently, Westinghouse Electric Corp., under contract to the FAA, manufactured the ASR-9, which uti-
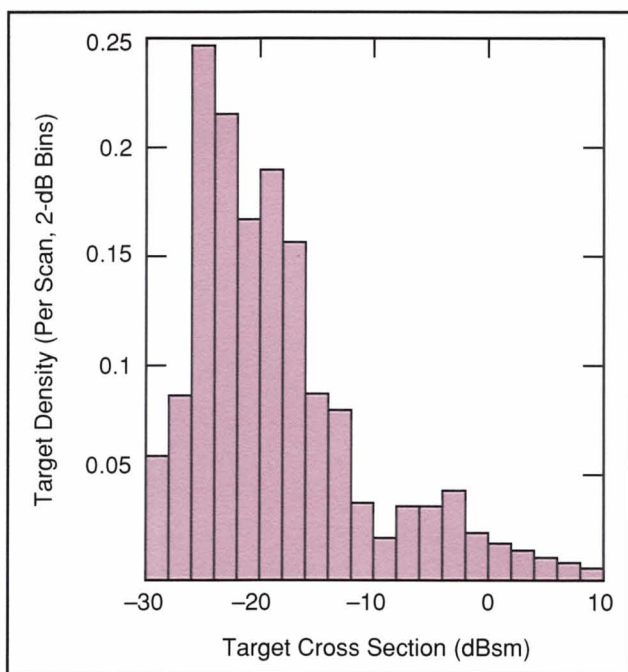

Fig. 6—Cross-section population densities for aircraft and birds (Burlington, Vt.). There is an overlap of the two populations in the region between −10 and 0 dBsm.
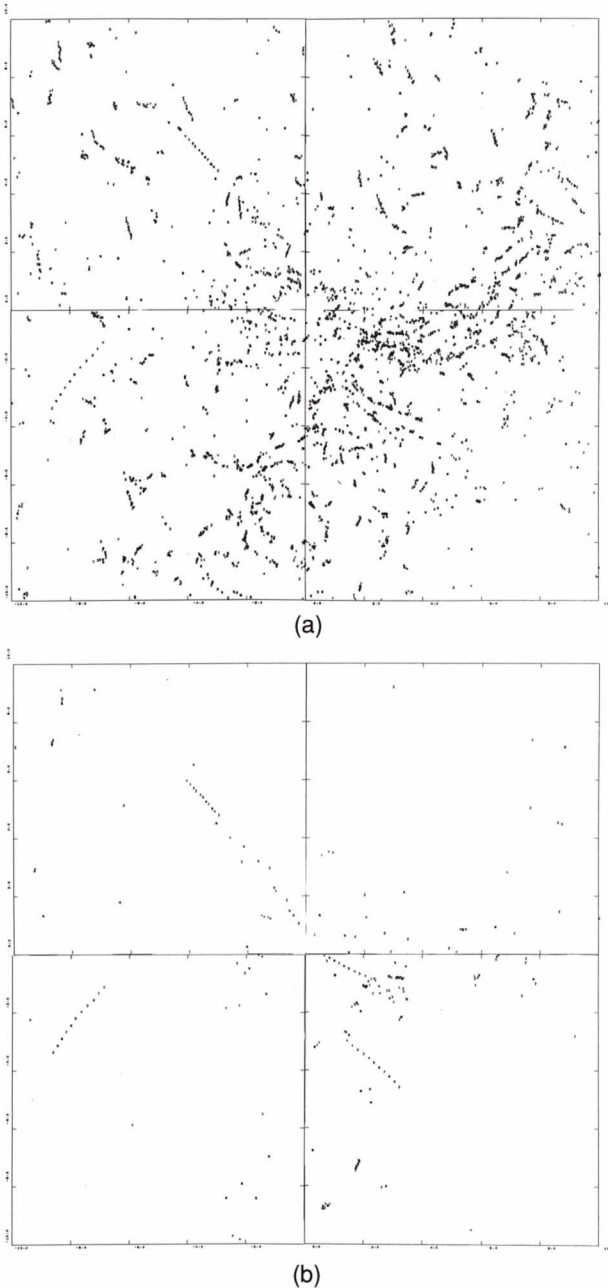
(a)

(b)

Fig. 7— Bird-echo processing. (a) Radar data before area thresholding. (b) Area thresholding removes undesirable bird echoes. The plots each represent an area of 20 nmi by 20 nmi.

lizes contemporary signal processing technology and a special-purpose tracking processor that was derived from the PMP. The salient results of Lincoln Laboratory tests of MTD and Westinghouse tests of ASR-9 follow.

Figure 8 gives an example of MTD performance in the intense ground-clutter environment

of Burlington. Figure 8(a) shows the cumulative reports before MTD tracker processing and Fig. 8(b) shows the same data after tracker processing. The false-alarm rate was typically less than one per scan and rose to less than 10 per scan under adverse conditions, e.g., when flocks of

(a)

(b)
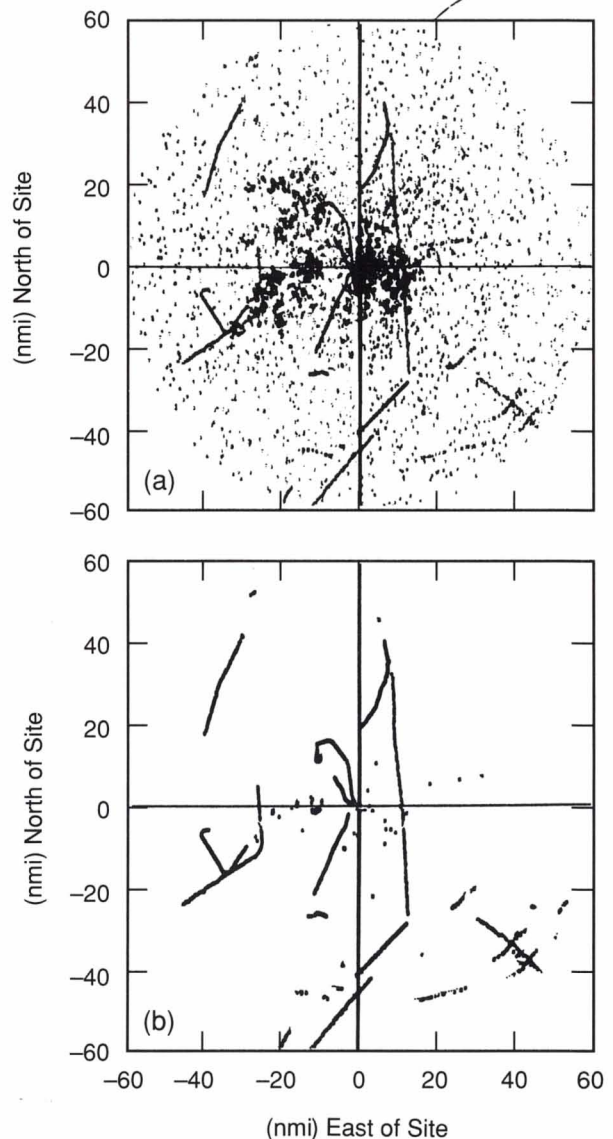
Fig. 8—An example of the tracker-processor stage of MTD-II. (a) Cumulative reports before tracker processing. The 100-scan plot, which constitutes eight minutes of radar data, illustrates the typical traffic present at the Burlington, Vt., airport. (b) Cumulative reports after tracker processing. MTD-II was able to achieve a false-alarm rate of less than one false alarm per scan. Under adverse conditions, a rate of less than 10 false alarms per scan is achievable.

370

birds were visible.

Figure 9 presents the tracker record of a small general-aviation aircraft whose backscattering cross section ranged from –3 dBsm to +8 dBsm [10]. The aircraft deliberately flew over large amplitude clutter to the southeast of Burlington, a region where clutter in range cells that exceeded 70 dB existed. Under such adverse conditions, MTD could not detect the target because of limitations imposed by the radar system stability. For traffic normally encountered in the area, however, the system's detection of targets was greater than 94%.

The one-standard-deviation azimuth error of MTD-II as well as of ASR-9 was measured to be 0.13°. The one-standard-deviation range error was measured to be 100 ft [12].

The first production model of ASR-9 was installed at Huntsville, Ala. The system, which has undergone extensive site adaptation and performance evaluation, was commissioned into operational service on 2 May 1989. The Huntsville site has a relatively benign ground-clutter environment. However, the location of the site is such that ground vehicular traffic from a number of roads is visible to the radar. As a result, maps of the visible roads had to be generated so that ASR-9 could use the information in editing the radar data.

The performance of the Huntsville ASR-9 represents a quantum improvement over existing digital radar target-detection systems. Figure 10, a plot of the output of ASR-9 for a period of about three minutes, includes the target detections of the Air Traffic Control Radar Beacon System (ATCRBS) for the same time period. As can be seen from the figure, the two systems have different strengths. Due to its elevation-beam pattern, ASR-9 is prone to losing targets at high elevation angles (> 45°) and short ranges (< 2 nmi). At longer ranges, however, ASR-9 can in many cases exceed the detection probability
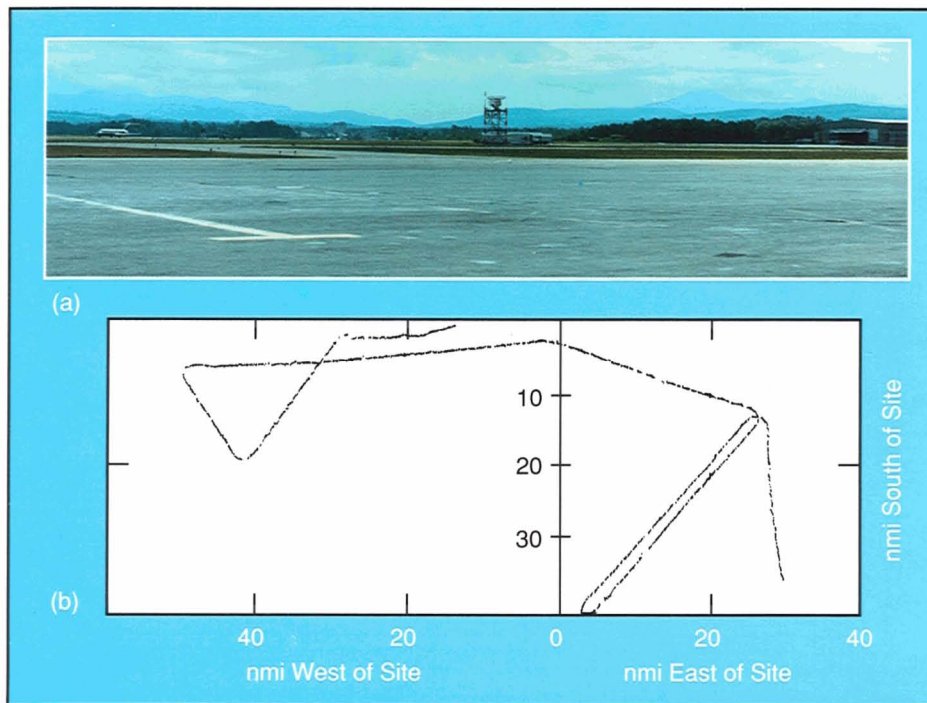

Fig. 9—(a) Hills surrounding the airport in Burlington, Vt., result in intense ground clutter. (b) The tracker output, obtained from a Cessna-172 flight test taken in the vicinity, demonstrates MTD-II's high probability of detection in a challenging environment. The probability detection for the 1-h track of the 3-dBsm target was 0.94.

of the beacon system, particularly in situations in which an aircraft's beacon antenna is shielded from interrogation.

Figure 10, which shows the ASR-9 operating with a false-alarm rate at or better than the system's designed rate of 1 false alarm per 4.7-s radar scan, demonstrates a target-detection capability on the same order as the beacon system. That is, during the test ASR-9 had a detection probability that exceeded 95% for the aircraft in the nominal coverage region. Because of ASR-9's low false-alarm rate, the integration of primary and beacon sensors is possible. Such integration provides near-perfect target-detection performance.

However, nominal conditions for radar observation do not occur every day. For example, environmental variables such as anomalous radar propagation due to extremes in the vertical atmospheric temperature and moisture profiles do occur. Small-scale weather echoes

Fig. 10—The performance of the Huntsville, Ala., ASR-9 radar as compared to the transponder-based Air Traffic Control Radar Beacon System (ATCRBS). This figure presents 30 radar scans of data. Targets detected by both ASR-9 and ATCRBS are plotted in green, targets detected only by ASR-9 are shown in yellow, and targets detected only by ATCRBS are depicted in red. Range rings are drawn at 10-nmi intervals.

also contribute to the number of false target reports. The ASR-9 radar, which is designed to adapt to difficult environments, should produce no more than 10 false reports per scan even under extreme conditions. To date, experience in Huntsville has supported this level of performance.

Weather Channel

A digital weather channel in ASR-9 supplants the wideband-video qualitative rendering of storm intensity that existed in the earlier airport primary radars. The weather channel provides superior performance by producing smooth, stable contours of storm intensity. Unlike the weather data produced by MTI, the ASR-9 contours are not biased by the following factors: the sensor's circuitry, circular polarization, antenna high-low beam selection, and sensitivity time control. In ASR-9, a programmable range-dependent threshold compensates for the above factors and reduces the estimate bias that occurs from the partial filling of the radar beam by the vertical extent of the storm. A set of four filters effectively eliminates ground clutter. The attenuating effect of these filters on storm echoes that have low radial velocities is mitigated by a ground-clutter map that was made on a clear day. The clear-day map can be used to select, on a range-cell-by-range-cell basis, the output of the least attenuating filter for each desired weather level. Spatial and temporal smoothing provides stable contours of precipitation regions. A brief description of the major functional modules follows.

Figure 11 contains a block diagram of the ASR-9 weather processor. (Details of the processor's antenna, the RF switching of the received signal from the high and low antenna beam, and the selection of linear vertical or circular polarization have been omitted.) Digitized quadrature video signals pass through four parallel clutter filters: one all-pass and three notch type. The filters are designed to remove scan-modulated clutter that has an intensity ranging from 12 dB to 49 dB. For that range of clutter intensity, the block-staggered PRF of the ASR-9 provides for the processing of 8 or 10 pulses to produce filters
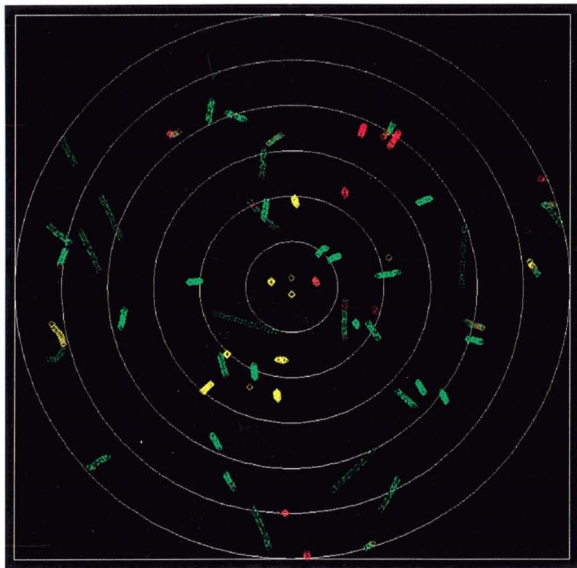
Primitive
Detections

Fig. 11—Block diagram of the ASR-9 weather processor, whose output is
a narrowband data stream capable of transmissions via telephone lines.

that have rejection bands centered on zero and
falling between 2 m/s and 7 m/s. To choose the
least-attenuating filter for each cell, the weather
processor uses both the echo-intensity and
ground-clutter map data. The all-pass filter is
selected for clutter-free regions or for regions of
high-level weather intensity.

The weather processor then subjects the
filtered output from each cell to thresholds
that are referenced to the six National Weather
Service (NWS) levels [13–15] of Table 2. The
thresholds are adjusted to compensate for dif-
ferent factors such as range dependence, beam
filling [1, 14], polarization, and high-low beam
[14, 15].

Rapid scanning of the radar antenna and/or
fluctuations of the weather echoes can lead to
noisy storm-intensity estimates for a single
resolution cell. Therefore, the single-cell thresh-
old crossings are smoothed over 1 nmi and the
highest level of 8 of the 16 resolution cells is
passed on for further temporal and spatial
smoothing. Six consecutive antenna scans are
median filtered to provide temporal smoothing.
Spatial smoothing is carried out on two levels.
The first is carried over adjacent echo clusters;
the second expands the weather contours
slightly to ensure that small regions of intense
reflectivity will not be obscured on the control-
ler's display.

The performance of the weather channel has
undergone simulation analysis, emulation, and
in situ validation. The simulation analysis by
M.E. Weber [13] showed that under a variety of
meteorological conditions, the weather channel
provides accurate representation of the NWS
level. In addition, Weber demonstrated that the
broad range of intensities encompassed by each
of the six levels would lead to an accuracy of
most of the estimates to within one NWS level.

The emulation facility (FL-3) developed for
the investigation of wind shear [16] was used
to acquire time-series data that were processed
by the algorithms described above. When the
weather channel of the first ASR-9 was checked
against observations made by both the emula-
tion-facility radar and a pencil-beam Doppler
weather radar, we found that the channel pro-
vided appropriate representations of storm in-
tensity for a variety of storms.

Figure 12, a time-lapse plot of data generated
by the ASR-9 weather channel, shows the pro-
gression of a squall line. Five of the six NWS
levels occurred in the storm.

The ASR-9 weather data appear on the air
traffic controller's display in either a discrete
(Fig. 13[a]) or summation (Fig. 13[b]) mode. Both
modes and ASR-9's six-level-selection features
provide air traffic controllers with accurate and
timely weather information that can be used to

Table 2. National Weather Service (NWS) Levels		
NWS Level	dBz Range	Rainfall Category
1	16 to 30	Mist to light
2	30 to 41	Moderate
3	41 to 46	Heavy
4	46 to 50	Very heavy
5	50 to 56	Intense
6	>56	Extreme (hail)

manage the traffic flow to gate posts, which are typically 40 mi from an airport. The features are also helpful in effecting tactical control of aircraft arrivals and departures in the presence of hazardous weather [14].

System Improvements

The original design concept, embodied in MTD-II, did not provide for the elimination of range-ambiguous aircraft echoes, i.e., aircraft flying within the detection capability of the radar but beyond the unambiguous range. This shortcoming resulted from a design decision to eliminate range-ambiguous fixed clutter. Another problem may arise when nearby automobile traffic is present. The following sections describe corrective measures that have been implemented or proposed.

Range-Ambiguous Targets

The problem of detecting range-ambiguous aircraft was solved in ASR-9 by applying microstagger to the pulse-repetition interval. Microstagger increases the pulse-repetition interval by two range cells (300 m) so that echoes from the first and subsequent ambiguous-range intervals are asynchronous with one another. By using this asynchronization, we can eliminate the range-ambiguous echoes of the aircraft.

Figure 14(a) is an example of range-ambiguous echoes. Note that the echoes (shown in magenta) produce nearly radial tracks that result from the extended azimuthal coverage of the radar beam. Figure 14(b) shows how microstagger can effectively remove range-ambiguous echoes. In mountainous regions where range-ambiguous clutter can occur, it may be necessary to revert to a nonstagger-
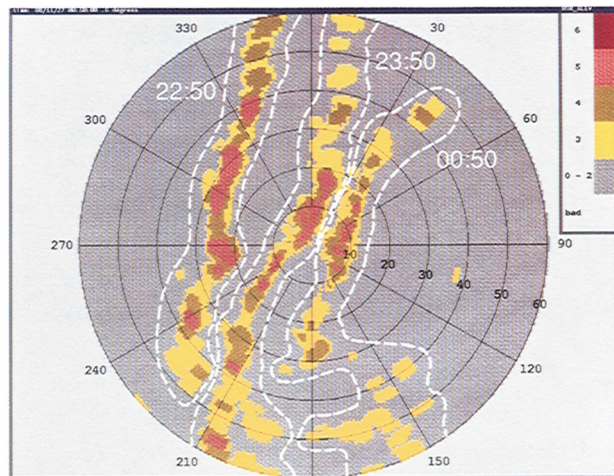
Fig. 12—ASR-9 weather-channel output showing the progression of a squall line. Color is used to denote the six National Weather Service (NWS) levels of Table 2. Note that five of the six levels were present in the storm.
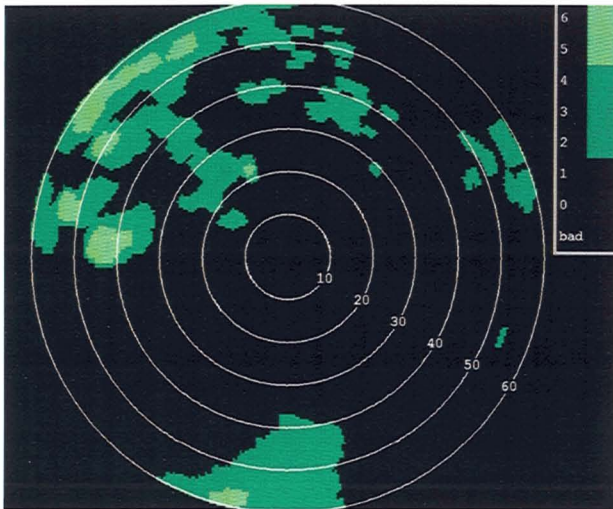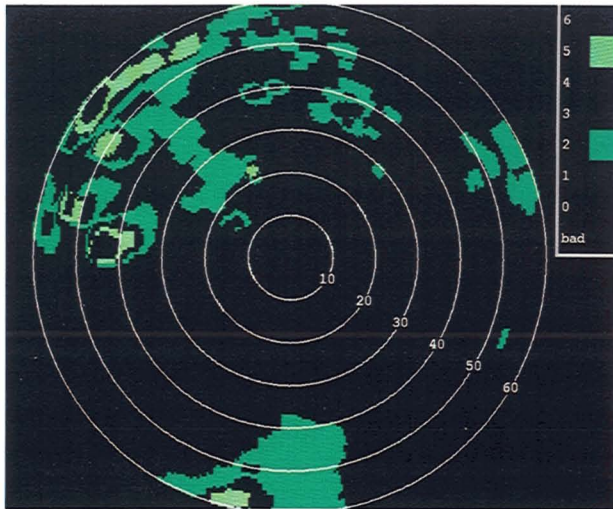
Fig. 13—*ASR-9 weather reports as displayed by the Automated Radar Terminal System (ARTS). An air traffic controller can select either the (top) discrete or (bottom) summation mode to obtain a comprehensive plan view of the weather situation.*

ed pulse-repetition interval in order to eliminate the clutter. An extended clutter map will aid the selection of the appropriate signaling strategy.

Vehicular Traffic

The ASR-9 radar has a subclutter visibility of about 45 dB; i.e., the radar can detect a moving target with an amplitude about 45 dB less than the amplitude of the ground clutter returns in the same range-azimuth cell. However, high

subclutter visibility is often more of a problem than a benefit in controlling the false-alarm rate. A striking example of this effect occurs when automobiles and other ground traffic are pres-
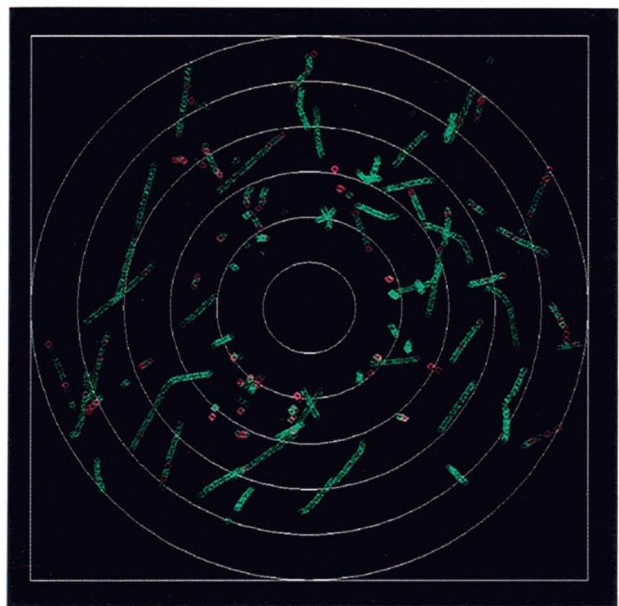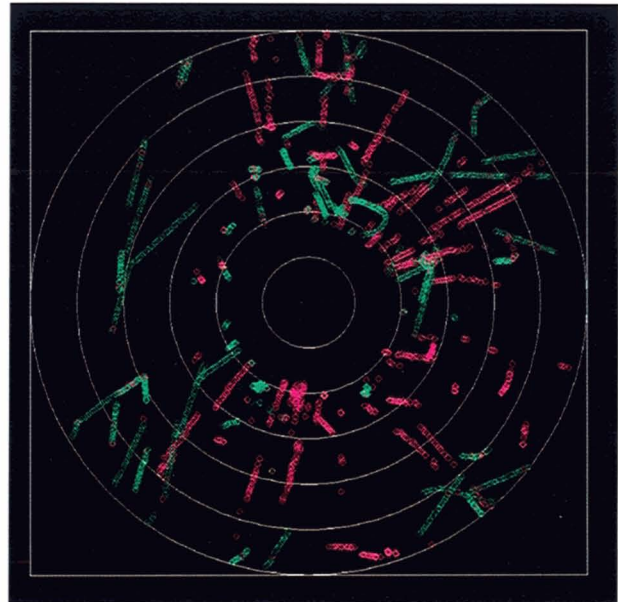
Fig. 14—*(top) Tracks of range-ambiguous aircraft detected with constant-pulse-repetition-frequency (PRF) blocks. The magenta markings indicate targets that have been detected in only one of the two radar PRFs. Most of these targets are false alarms caused by echoes received from aircraft at greater than the 60-nmi instrumented range of the radar. (bottom) The range-ambiguous echoes have been eliminated with microstagger.*

ent. When roads are visible, air traffic controllers using current radars are aware that some target reports may result from ground vehicles. Between the limited subclutter visibility of current radars and the lack of automated target detection and tracking, these returns are usually considered to be relatively minor annoyances rather than a significant limitation on system performance. In the case of new high-performance radars, the situation becomes more critical.

The increased subclutter visibility of the ASR-9 leads to the detection of surface vehicles within the line of sight of the radar. In fact, one aspect of most of the class of false alarms uncovered by the new signal processing technology is that, with the exception of bird-target reports, the false alarms are produced by scatterers on the ground. The presence of bird reports can be identified through the careful
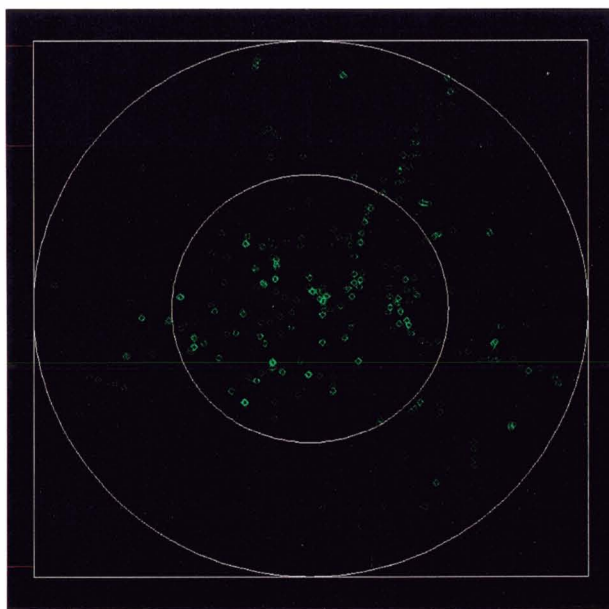

Fig. 16—A simulation of the false-alarm environment at Huntsville, Ala., for the same period as Fig. 15. This simulation was performed with data taken by the Lincoln Laboratory FL-3 test radar, whose site was about 0.5 nmi from the ASR-9. The use of the FL-3 data allows a depiction of the expected false-alarm rate without automatic false-alarm removal techniques.

Fig. 15—A five-scan plot of the short-range-detection and false-alarm-rate performance of ASR-9 in Huntsville, Ala. This plot shows on an expanded range scale the same data as the first five scans of Fig. 10. (Targets detected by both ASR-9 and ATCRBS are plotted in green, targets detected only by ASR-9 are shown in chartreuse, and targets detected only by ATCRBS are depicted in orange.) In ASR-9, false alarms are removed with interference detection, fixed site-dependent censoring maps, adaptive amplitude thresholding, and scan-to-scan correlation.

assessment of target-amplitude statistics. However, this technique is not effective against ground targets such as trucks that elicit target reports that have both amplitudes and Doppler frequencies comparable to those of aircraft.

To date, MTD-II and the ASR-9 algorithms have been capable in controlling false alarms due to ground traffic (Fig. 15). Before the data of Fig. 15 were subjected to postprocessing, there were more than 100 false reports per scan. The false reports were removed with a site-specific map, which contained information about visible roads.

Figure 16 is a reproduction of the results of an ASR signal processor simulation. (The data are taken from wind-shear experiments with the Lincoln Laboratory FL-3 radar [17], which is a modified ASR-8 radar used for the development of ASR signal processing algorithms.) We processed the recorded time-series data to simulate the performance of an MTD-like processor in the same environment and time period as the con-

ditions under which the ASR-9 data shown in Fig. 15 were collected. (To highlight the vehicular traffic, we used only the first 20 nmi of the data.) Fig. 16 exhibits a large number of false-target reports, many of which come from automobile and truck traffic. In the ASR-9 plot (Fig. 15), these reports were removed at the signal processor level by a site-dependent target-censoring map that was carefully hand compiled to screen those roads which are visible to the radar.

We should point out that Huntsville is far from an extreme case with respect to vehicular traffic. Hence this technique will be further tested as ASR-9 installations proceed at other airports. Whether the use of target-censoring maps will prove acceptable at all sites remains questionable. The possibility exists that at some sites important aircraft-coverage regions might occur over dense ground-traffic areas. This situation would prevent the simultaneous achievement of both a very low false-alarm rate and an acceptable probability of detection.

Thus it is desirable to deal with the problem of automobile traffic in a more fundamental way. One approach under evaluation is the addition of a single-target height-measurement capability to the radar. This approach places targets that are due to ground-based returns into elevation-angle classes that can be suppressed without any degradation to the aircraft-detection ability of the system.

In Huntsville we began to explore the use of elevation angles to differentiate between ground-based and airborne targets. We investigated whether a vertical interferometer consisting of two radar receiving feed horns could accurately measure the elevation angles.

The ASR-8 and ASR-9 radars have two feed horns mounted on rotating antennas. The feed horn associated with the lower beam is always used to transmit, and either of the two feeds can be used for reception. In normal operation the receiver is simply range switched between the two horns. The higher-beam horn is used at shorter ranges to provide about 12 db of additional ground-clutter rejection. The lower-beam horn is used at longer ranges (i.e., at ranges greater than about 12 nmi) in which the low-

angle coverage is more important.

In contrast to the configuration used in the ASR-8 and ASR-9, the FL-3 radar has two separate receiver chains and can thus record video simultaneously from both antenna feeds. The simultaneous signals can be used to determine a target's elevation in the following way. By considering the complex cross-spectrum of the two time series, we can take the cross-spectral phase at a particular frequency to be representative of the elevation of a target at that frequency, even in the presence of ground clutter or other targets with different velocities.

Figure 17 shows an example of the vertical-amplitude and phase-pattern measurements of the ASR-9 antenna. As might be expected, the relationship between the differential phase value and the elevation angle of the scatterer is generally monotonic. The slope of the differential phase curve is steepest at low elevation angles, and since the height-assignment accuracy of such a processor increases with increasing phase slope, the antenna should be capable of making accurate elevation-angle measurements of objects near the ground. For high signal-to-noise targets (20 to 30 dB) with the ASR-9 antenna, this accuracy should be better than ± 0.1° at low elevation angles.

The vertical-interferometer approach is basically a vertical-phase monopulse system. Consequently, the approach shares many of the drawbacks common to such systems—in particular, problems with the phase stability of such RF hardware as waveguides and rotary joints.

On the other hand, an important advantage of the vertical-interferometer approach is that it provides a means of identifying the received signal from the ground clutter itself. As the radar components drift slowly in time, the ground-clutter signal supplies a reference phase at each range and azimuth that can be tracked. This dynamic approach to obtaining a reference phase is also useful since it automatically accounts for variations in ground topography around the radar (Fig. 18).

We can design a radar processor so that its algorithms for signal processor thresholding
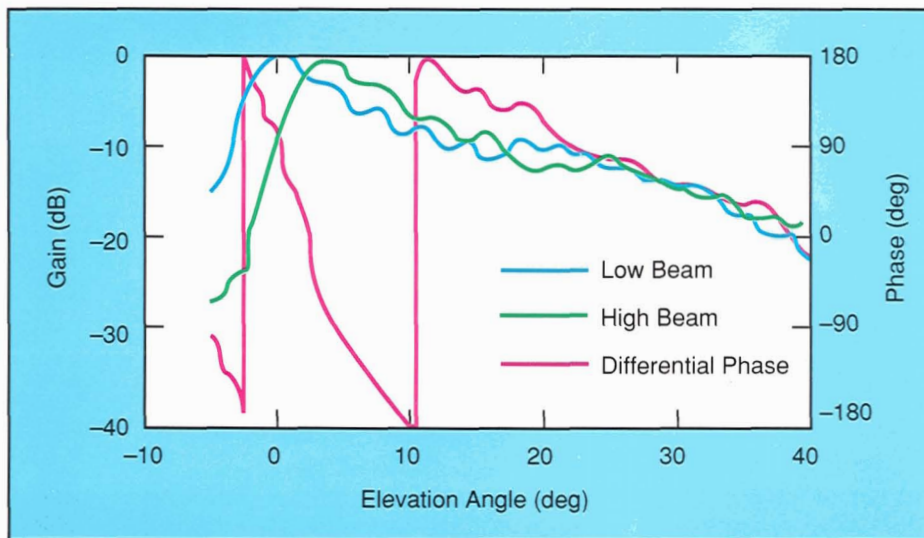
Fig. 17—Vertical amplitude and phase pattern of a production ASR-9 antenna. (The data were measured by Westinghouse Electric Corp. under contract to the FAA.)

select only those range-azimuth-Doppler threshold crossings which have a dual-beam cross-spectral phase that is not within some error tolerance of the local ground-return phase. Figure 19 shows an example of the simulation of such a processor from the FL-3 data set. The target plot demonstrates a greater than 90% reduction of false targets while it preserves the detection of nearly all of the genuine aircraft returns.

The results of the simulation demonstrate that with some increase in RF and signal processing complexity, vehicular traffic can be automatically eliminated with far less site-specific knowledge than was required by the ground-clutter-map method. The technique can also be extended to zero Doppler velocity in which, in superclutter conditions, the target signal is stronger than the clutter signal. Under these circumstances, the vertical-interferometer technique can provide better visibility than the zero-Doppler temporal CFAR thresholding currently employed.

Although the discussion in this article has concentrated on false alarms due to ground vehicles, the same processing strategy can potentially be used to remove false reports that result from finite-velocity clutter such as windblown vegetation.

Summary

MTD and its implementation in the production ASR-9 represent a significant advance in
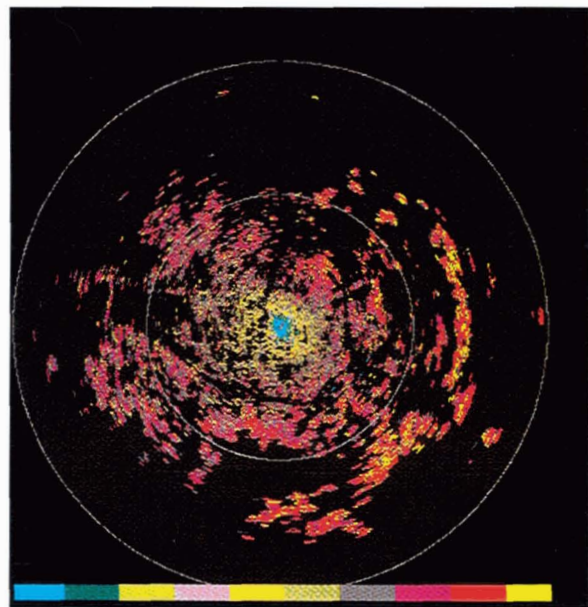

Fig. 18—A plot showing the apparent elevation angle of visible ground clutter as computed from the phase measured by the two vertical beams that were used as an interferometer. In this plot, the phase increases from the relatively large depression angle near the 60-ft FL-3 tower (note the blue colors) to higher elevation angles (shown in yellow) at longer ranges. The cross-spectral phase ranges from 0° (indicated by blue) to 100° (indicated by yellow).
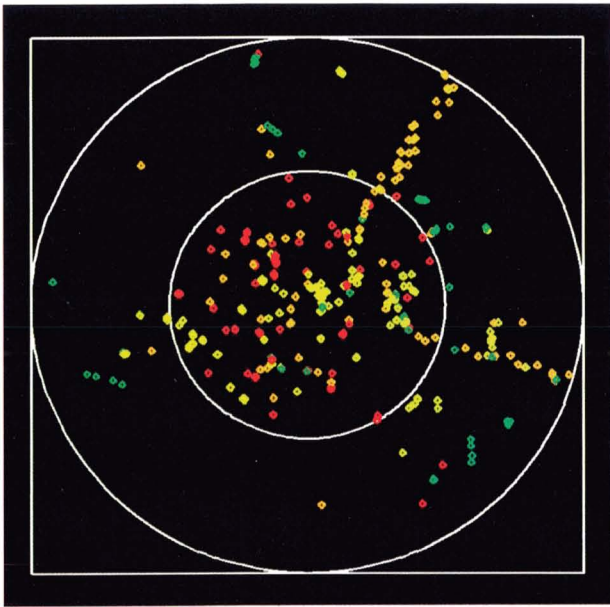
378

Fig. 19—Output of the FL-3-based ASR emulation system. (The data are from Fig. 16.) Note that false alarms due to interference by other radars (chartreuse), bird echoes (red), and ground vehicular traffic (orange) have been detected. Bird echoes are removed with area thresholding. Clutter resulting from surface vehicular traffic is removed with a phase-derived height estimate. Targets that survive all of the false-alarm tests are shown in green.

the surveillance of aircraft and weather that is required to support the automation of air traffic control. The low false-alarm rate of MTD's aircraft-detection algorithm can be improved further by adding the elevation-angle discriminant to reject ground traffic. A wind-shear detection capability that could also be incorporated to provide an at-the-airport measurement of hazardous radial wind fields is an additional topic of current investigation. In summary, the MTD and its enhancements will effectively serve in the future as the processing architecture for mechanically scanning airport primary radars.

Acknowledgments

References

1. J.W. Taylor, Jr. and G. Brunins, "Design of a New Airport Surveillance Radar (ASR-9)," *Proceedings of IEEE* **73**, 284 (1985).
2. C.E. Muehe, Jr. and L. Cartledge, "A High Performance, Low Cost, Air Traffic Control Radar," *Technical Note 1973-12*, Lincoln Laboratory (15 Feb. 1973), AD759179.
3. C.E. Muehe, "Concepts for Improvement of Airport Surveillance Radars," *Project Report ATC-14*, Lincoln Laboratory (26 Feb. 1973), AD75739.
4. C.E. Muehe, L. Cartledge, W.H. Drury, E.M. Hofstetter, M. Labitt, P.B. McCorison, and V.J. Sferrino, "New Techniques Applied to Air Traffic Control Radars," *Proceedings of IEEE* **62**, 716 (June 1974).
5. "Doppler Processing Waveform Design and Performance Measures for Some Pulsed Doppler and MTD Radars," *Ortung und Navigation Part 1*, p. 417 (Mar. 1981); *Part 2*, p. 2 (Jan. 1982).
6. W.H. Drury, "Improved MTI Radar Signal Processor," *Project Report ATC-39*, Lincoln Laboratory (3 Apr. 1975), FAA-RD-74-185.
7. C.E. Muehe, "Digital Signal Processor for Air Traffic Control Radars," *IEEE/NEREM 1974, Part 4: Radar Systems and Coponents*, Boston, 28–31 Oct. 1974, p. 73.
8. C.E. Muehe, P.G. McHugh, W.H. Drury, and B.G. Laird, "The Parallel Microprogrammed Processor (PMP)," *IEE 1977 Intl. Radar Conf.*, London, 25-28 Oct. 1977, p. 97.
9. C.E. Muehe, "Advances in Radar Signal Processing," *IEEE ELECTRO/74 Professional Program*, Boston, 11–14 May 1976, p. 1.
10. J.R. Anderson and D. Karp, "Evaluation of the MTD in a High-Clutter Environment," *IEEE 1980 International Radar Conference*, Arlington, VA, 28–30 Apr. 1980, p. 219.
11. "Airport Surveillance Radar (ASR-9)," *Department of Transportation/Federal Aviation Administration Specification* (1 Oct. 1986), FAA-E-2704B.
12. D. Karp and J.R. Anderson, "Moving Target Detector (Mod II) Summary Report," *Project Report ATC-95*, Lincoln Laboratory (3 Nov. 1981), ADA114709.
13. M.E. Weber, "Assessment of ASR-9 Weather Channel Performance: Analysis and Simulation," *Project Report ATC-138*, Lincoln Laboratory (31 July 1987), FAA/PM-86-16.
14. D.C. Puzzo. S.W. Troxel, M.A. Meister, M.E. Weber, and J.V. Pieronek, "ASR-9 Weather Channel Test Report,"

Project Report ATC-165, Lincoln Laboratory (1989), FAA-PM-86-38.

15. S.W. Troxel. "ASR-9 Weather Channel Test Report, Executive Summary," *Project Report ATC-168*, Lincoln Laboratory (3 May 1989), DOT/FAA/PS-89/6.

16. M.E. Weber and T. Noyes. "Wind Shear Detection with Airport Surveillance Radars," *Lincoln Laboratory Journal* **2**, 511 (1989).

17. M.E Weber and T.A. Noyes, "Low Altitude Wind Shear Detection with Airport Surveillance Radars: Evaluation of 1987 Field Measurements," *Project Report ATC-159*, Lincoln Laboratory (31 Aug. 1988), FAA/PS-88/10.

MELVIN L. STONE is the Associate Group Leader of the Air Traffic Surveillance Group, which develops technology for current and next-generation airport-surveillance radars (ASR) and airport surface detection equipment (ASDE). Mel received a B.S. degree in electrical engineering from MIT in 1951. He participated in the development of weather radar techniques as a member of the staff of the MIT Dept. of Meterology Weather Radar Laboratory from 1948 to 1951. Since he joined Lincoln Laboratory 37 years ago, Mel's research interests have included weather radar, HF ground-wave backscatter from the sea and aircraft, lunar albedo at UHF, auroral backscatter from UHF through L-band, and ionospheric effects caused by burning missiles. He developed a 400-kW X-band radar used in the Fourth Test of General Relativity. Mel was also leader of the group that developed an air-to-ground moving-target radar, the progenitor of the U.S. Air Force/Army Joint Standoff Target Attack Radar System (JSTARS). He is a member of the IEEE, AGU, Sigma Xi, and Eta Kappa Nu.

JOHN R. ANDERSON is an associate professor of the Department of Meteorology and associate director of the Space Science and Engineering Center at the University of Wisconsin in Madison. The system engineer for the MTD-II radar, John has been involved in the development of radar signal and data processing algorithms. He is currently involved in the development of signal processing and post-processing algorithms for Doppler weather radars designed for the detection of thunderstorm-generated aviation hazards. His meteorological research projects include the study of the dynamics of the tropical atmosphere and the extension of 4-D data-assimilation techniques to the problem of integrating Doppler radar data with thunderstorm-scale prediction models for the purpose of short-term forecasts of aviation hazards near airports. John received a S.B. in physics and S.M. in meteorology from MIT in 1976 and 1982, respectively, and a Ph.D. in atmospheric sciences from Colorado State University in 1984.